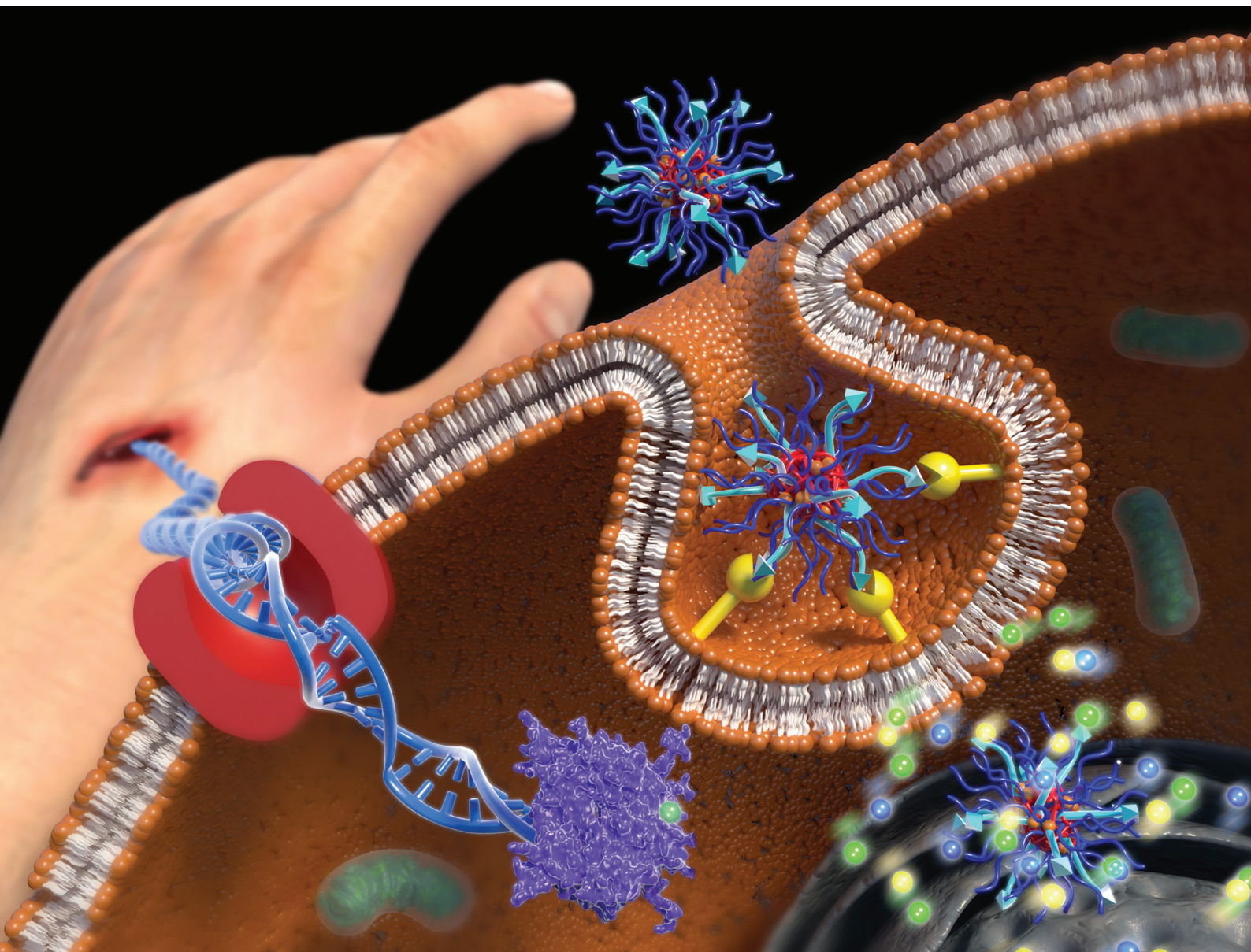


Biomaterials Science

Volume 11
Number 2
21 January 2023
Pages 345-692

rsc.li/biomaterials-science




ISSN 2047-4849

PAPER

Chul-Su Yang, Jin Woong Kim *et al.*
Fibroblast-targeting polymeric nanovehicles to enhance
topical wound healing through promotion of PAR-2
receptor-mediated endocytosis

Cite this: *Biomater. Sci.*, 2023, **11**, 450

Fibroblast-targeting polymeric nanovehicles to enhance topical wound healing through promotion of PAR-2 receptor-mediated endocytosis†

Yousong Lee,^a Seulgi Kim,^a Jihye Seo,^a Hyo Keun Kim,^b Yeong Pin Han,^b Eun Ju Park,^c Jin Oh Park,^c Chul-Su Yang*^b and Jin Woong Kim *^a

The level of collagen production critically determines skin wound contraction. If an intelligent skin drug delivery technology that enables collagen production in a specific wound skin area is developed, a breakthrough in wound healing treatment would be expected. However, such an intelligent drug delivery technology has not yet been developed as much as in the field of anticancer therapy. In this study, we propose a smart drug delivery system using polymeric nanovehicles (PNVs), in which the periphery is conjugated with a fibroblast-targeting collagen-derived peptide, KTTKS (Lys-Thr-Thr-Lys-Ser). We showed that surface engineering of PNVs with simultaneous PEGylation and peptide patching improved the dispersibility of PNVs, while promoting selective cellular uptake to fibroblasts via PAR-2 receptor-mediated endocytosis. *In vitro* collagen production and *in vivo* wound healing assays revealed that curcumin-loaded fibroblast-targeting PNVs significantly enhanced collagen production and wound healing activities, thus promising effective skin tissue regeneration.

Received 25th August 2022,
Accepted 20th November 2022

DOI: 10.1039/d2bm01357f

rsc.li/biomaterials-science

Introduction

The wound healing process involves four phases: hemostasis, inflammation, proliferation, and remodeling.^{1,2} Fibroblasts are deeply involved in all phases of wound healing, secreting growth factors, cytokines, collagens, and other extracellular matrix (ECM) components.^{3–6} Therefore, they need to proliferate at the wound site to enhance the therapeutic effect during healing of the wound tissue. To this end, a variety of self-assembling biomolecules and nano biomaterials have been extensively investigated, with the aim of developing drug delivery systems.^{7–10} However, these systems not only work on fibroblasts, but affect other cells as well, which eventually lowers the wound healing efficiency.¹¹ Therefore, it is necessary to develop a technology that can selectively deliver wound healing drugs to fibroblasts. For site-specific drug delivery, bio-ligands including peptides, antibodies, and other proteins

have been conjugated to drugs or drug carriers.^{12–15} In skin tissue engineering, particularly, it is known that some ECM component-derived peptides exhibit specific affinity to the receptors on the skin cells.¹⁶ For example, a collagen-derived peptide conjugated on a drug carrier induces its endocytosis into the target cell sites through interaction with integrin receptors ($\alpha_1\beta_1$, $\alpha_2\beta_1$, $\alpha_{10}\beta_1$, and $\alpha_{11}\beta_1$)¹⁷ or non-integrin receptors such as discoidin domain receptors,¹⁸ mannose receptors,¹⁹ and CD44.²⁰ In particular, a type-1 collagen sub-fragment with the minimum necessary sequence, KTTKS, can interact with fibroblasts.^{21–24} This ligand–cell interaction-mediated delivery system enables better localization of drug molecules at the target cell sites, lowering immunogenicity and cytotoxicity.^{25,26}

Based on this understanding of the underlying wound healing mechanism, this study proposes an active drug delivery system established using fibroblast-targeting peptide (KTTKS, Lys-Thr-Thr-Lys-Ser)-conjugated polymeric nanovehicles (PNV_{KTTKS}) for wound healing applications. The key to our approach is to promote receptor-mediated endocytosis^{27,28} by inducing PNVs to selectively target the proteinase-activated receptor (PAR-2) present only on the cell membrane of fibroblasts.^{22–24} The PNVs were prepared by co-assembly of amphiphilic poly(ethylene oxide)-*block*-poly(ϵ -caprolactone) (PEO-*b*-PCL) with a mannosylerythritol lipid (MEL)-maleimide linker.²⁹ We verified that the KTTKS containing a cysteamide

^aSchool of Chemical Engineering, Sungkyunkwan University, Suwon 16149, Republic of Korea. E-mail: jinwoongkim@skku.edu; Tel: +82 31 290 7346

^bDepartment of Molecular & Life Science and Center for Bionano Intelligence Education and Research, Hanyang University, Ansan 15588, Republic of Korea. E-mail: chulsuyang@hanyang.ac.kr; Tel: +82 31 436 8137

^cDeabong Life Science Co., Incheon 21697, Republic of Korea

† Electronic supplementary information (ESI) available. See DOI: <https://doi.org/10.1039/d2bm01357f>

at the terminal sequence was covalently tagged with the MEL linker through a thiol–maleimide reaction.^{29,30} The periphery of PNV_{KTTKS} was decorated with PEO chains and KTTKS; the former increases the dispersion stability of PNVs through a favorable chain conformation, while the latter must be exposed at the surface rather than the PEO chain for fibroblast targeting. For effective wound healing, we identified how to engineer the PNV_{KTTKS} surface. We quantitatively confirmed the specificity of PNV_{KTTKS} to fibroblasts in the skin cell mixture. Finally, we systematically verified to what extent fibroblast targeting contributed to the improvement of wound healing performance.

Materials and methods

Materials

Two types of PEO-*b*-PCL were supplied by Mizon (Korea): one with a short PEO block of 2000 g mol⁻¹ and the other with a long PEO block of 5000 g mol⁻¹ while fixing the PCL block with 2000 g mol⁻¹. MEL was supplied by DK Bio (Korea). KTTKS was synthesized with cysteamide conjugated at the C-terminus and supplied by Peptron (purity of >90%, Korea). Anhydrous methylene chloride, pyridine, *N,N*-diisopropylethylamine, 4-nitrophenylchloroformate, *N*-(2-aminoethyl) maleimide trifluoroacetate salt, curcumin, and Nile red were purchased from Sigma Aldrich (USA). Tetrahydrofuran (THF) (purity >98%, TCI, Japan) was used as a removable solvent. Texas Red-1,2-dihexadecanoyl-*sn*-glycero-3-phosphoethanolamine (DHPE) and 4,6-diamidino-2-phenylindole (DAPI) were purchased from Thermo Fisher Scientific (USA). Human dermal fibroblast (HDF) cells were purchased from the American Type Culture Collection (ATCC, USA), and SK-MEL-28 cells and HaCaT cells were purchased from the Korean Cell Line Bank. Dulbecco's modified Eagle's medium (DMEM, Welgene, Korea) used was of reagent grade. Fetal bovine serum (FBS), penicillin–streptomycin, and phosphate-buffered saline (PBS) solution were supplied by GIBCO-Thermo Fisher Scientific (USA). Double-distilled deionized (DI) water was used for all the experiments.

Fabrication of PNV_{KTTKS}

We synthesized the MEL-maleimide linker for the conjugation of KTTKS with bare PNVs by following the protocol of our previous study (ESI, Fig. S1†).²⁹ To produce PNV_{KTTKS}, PEO-*b*-PCL (1% w/w) and MEL-maleimide linker (0.2 mg mL⁻¹) were completely dissolved in THF *via* sonication for 10 min at 40 °C and collected in a round-bottomed flask. In the case of the wound healing drug, curcumin (0.01% w/w against total mass) was dissolved in the solution. Subsequently, DI water (9.9 mL) was added dropwise to the mixture while stirring using a syringe pump (Pump 11Elite, Harvard Apparatus, USA) at a flow rate of 100 μL min⁻¹. After the formation of the nanovehicles, THF was completely removed from the dispersion by evaporation at 40 °C for 20 min. The excess drug was removed by filtration through a 0.1 μm syringe filter. Then, controlled amounts of

KTTKS were added to the dispersion while gently stirring at room temperature for 12 h. The concentration of PNV_{KTTKS} was adjusted to 1% w/w against the total dispersion mass.

Characterization of PNV_{KTTKS}

The particle sizes and zeta potentials of PNVs and PNV_{KTTKS} were measured by dynamic light scattering (ELS-Z, Otsuka Electronics, Japan) at 25 °C. The morphology of PNVs and PNV_{KTTKS} was observed under an energy-filtering transmission electron microscope (LIBRA 120, Carl Zeiss, Germany). To determine the encapsulation efficiency of curcumin in the curcumin-loaded KTTK-conjugated PNVs (CPNV_{KTTKS}), 1 mg of freeze-dried CPNV_{KTTKS} was dissolved in 1 mL of methanol. For quantification, a standard calibration curve was plotted using standard concentrations of curcumin dissolved in methanol. Spectrophotometric measurements were obtained from the absorbance at 420 nm of the UV–visible spectra (Lambda 365, PerkinElmer, USA). The encapsulation efficiency (%), determined by comparing the curcumin mass in the CPNV_{KTTKS} against the initially added curcumin mass, was measured to be 85–90% (Fig. S2†).

Cell culture and viability assay

The cells were incubated in the culture medium, DMEM supplemented with 10% FBS and 1% penicillin–streptomycin, at 37 °C under a humidified atmosphere containing 5% CO₂. The *in vitro* cytotoxicity of CPNV_{KTTKS} was evaluated using an EZ-Cytox kit (EZ-3000, Dogen, Korea). Curcumin dissolved in dimethyl sulfoxide (DMSO) was used, and the concentration of DMSO in the culture medium was tuned to be less than 0.1% v/v. HDF cells were seeded at a density of 4 × 10³ cells per well in a 96-well plate and incubated overnight. After removal of the cell media, the cells were exposed to a series of CPNV_{KTTKS} samples diluted in DMEM at different concentrations for 24 h. After washing with PBS, 100 μL of the EZ-Cytox solution was added to each well. The plate was incubated for 2 h and the absorbance was measured at 450 nm using a microplate reader (Spark, Tecan, Switzerland).

Analysis of cellular uptake

HDF cells were seeded at a density of 4 × 10³ cells per well in a 96-well plate and incubated overnight. Nile red-loaded PNV_{KTTKS} was diluted in the culture medium. After removing the media from the cell culture plate, the cells were incubated with 100 μL of dispersed PNV_{KTTKS}. After washing the dispersed samples twice with PBS, the fluorescence was measured at 580/670 nm (excitation/emission) using a microplate reader. To demonstrate the fibroblast-specific cellular delivery of PNV_{KTTKS}, HDF, SK-MEL-28, and HaCaT cells (5 × 10⁴ cells per well) were co-cultured in a 6-well plate. They were incubated with Texas Red-DHPE-*co*-assembled PNV_{KTTKS} for 6 h. After washing with PBS, coverslips with cultured cells were fixed with 4% formaldehyde for 15 min and washed twice with PBS. For visualization of cell nuclei, the cell culture plates were treated with DAPI solution diluted with PBS for 20 min. The DAPI solution was then washed away with PBS, and the fluo-

rescence images were obtained using an inverted fluorescence microscope (Axio Vert.A1 Bio, ZEISS, Germany).

Determination of curcumin release

The curcumin release from CPNV_{KTTKS} was determined using the dialysis method.³¹ CPNV_{KTTKS} (1 mL), or free curcumin dissolved in DMSO (as control), was diluted with the release medium (PBS containing 5% v/v Tween-80). The concentration of curcumin in the test sample was adjusted to 0.5 mg mL⁻¹ and then packed in a dialysis tubing (MWCO: 3500 Da, Fisher Scientific, USA). The dialysis tubing was immersed in 100 mL of the release medium and continually stirred at 300 rpm at 37 °C. At particular time intervals, 1 mL of the release medium was collected and replaced with an equal volume of pre-warmed fresh buffer. The collected samples were stored at -20 °C until analysis. Subsequently, the concentration of the drug released was determined by measuring absorbance at 420 nm using a microplate reader.

Quantification of collagen synthesis stimulation

HDF cells seeded at a density of 4 × 10³ cells per well in a 96-well plate were incubated for 24 h and then treated with CPNV_{KTTKS} diluted with DMEM ([curcumin] = 5 μM). Next, the cells were washed with PBS and fixed *in situ* with ice-cold 70% ethanol. After the ethanol solution was removed, each well was washed with DI water. The cells were then treated with a Sirius red-picric acid solution and incubated overnight at 4 °C with gentle agitation. The unbound dye was removed by gently rinsing the fixed cells with DI water. This process was repeated until the residual unbound dye was removed from the bottom of each well. The cells were then treated with 1 N NaOH at room temperature with gentle agitation for 10 min to dissolve the collagen dye complex and ensure thorough mixing. Finally, the absorbance was measured at 540 nm using a microplate reader.

Western blot analysis

HDF cells seeded at a density of 1 × 10⁵ cells per well in a 6-well plate were incubated for 24 h and then treated with CPNV_{KTTKS} diluted with DMEM ([curcumin] = 5 μM). Next, the cells were washed with PBS, lysed in a RIPA buffer (CELL BIOLABS, USA) containing a protease inhibitor (Cell Signaling Technology, USA), and centrifuged at 13 500 rpm (12 300g) for 5 min at room temperature to recover the supernatant. The protein concentrations were determined using a BCA kit (Takara, Japan). The cell lysate samples (25 μg of protein) were subjected to a 10% SDS-PAGE gel (TGX™ Precast Midi Protein Gel, Bio-Rad, USA), transferred onto polyvinylidene fluoride membranes (Millipore, USA), and blocked with 5% non-fat milk in Tris-buffered saline containing 0.2% Tween 20 (TBS-T) for 1 h at room temperature. The membranes were then incubated overnight at 4 °C with anti-MMP-2 (cat. no. 4022S; Cell Signaling Technology, USA), anti-MMP-9 (cat. no. 3852S; Cell Signaling Technology, USA), anti-GAPDH (cat. no. Sc-47724; Santa Cruz Biotechnology, USA) and anti-ACTIN (cat. no. Sc-47778; Santa Cruz Biotechnology, USA) followed by incubation

with horseradish peroxidase (HRP)-conjugated goat anti-rabbit IgG (Abcam, UK) and HRP-conjugated goat anti-mouse IgG (Santa Cruz Biotechnology, USA) secondary antibodies at room temperature for 1 h. Proteins were visualized using an enhanced chemiluminescence kit (ATTO, Japan). The reactive bands were detected with an Odyssey® infrared imaging system (ImageSaver6, ATTO, Japan) and the density of the blots was measured using a CS Analyzer 4 (ATTO, Japan).

In vivo wound healing assay

Normal 6–8 week old male C57BL/6 mice were used for the *in vivo* experiment. First, the mice were treated under isoflurane anesthesia. Full-thickness skin injuries were then prepared by removing a round 6 mm diameter section using a biopsy punch. Then, curcumin, CPNV, and CPNV_{KTTKS} were used for treatment of the dorsal wound surface. The concentration of curcumin was fixed at 200 μM. The mice were maintained in a single cage for observation after surgery and recovery from anesthesia. Photographs of the wound region were taken during 12 days to visualize changes in the wound size over the healing period. The percentage of wound was determined by the percentage of wound area change against the original wound area. All animal experiments were approved by the Institutional Animal Care and Use Committee of Hanyang University (protocol 2021-0027) and conducted in accordance with the ethical protocol provided by the Korean Ministry of Health and Welfare.

Histology

For immunohistochemistry of tissue sections, after 12 days of treatment, the animals were sacrificed with an overdose of anesthetics and the wound areas were removed. The samples were immediately fixed using 10% buffered formalin embedded in paraffin. Paraffin sections (4 μm) were cut and stained with hematoxylin and eosin (H&E) or Masson's trichrome (MT). All images were examined under a digital microscope. The histologic scores were made from 20 random fields per section from each specimen,⁴¹ including the degree of epithelialization (absence or presence of epithelial covering, number of epithelial cell layers, crusting, spongiosis, intraepithelial inflammatory cells and blistering), granulation tissue and collagen matrix organization (adipose tissue substitution as an index of impaired wound closure, loose connective tissue or dense eosinophilic collagen matrix, edema, hemorrhage, degree of inflammation, number and organization of fibroblasts as well as their morphologic characteristics such as a plumped, spindle, or stellate-morphology as indices of activity), inflammatory infiltrates (number of inflammatory cells and their localization such as perivascular or intravascular inflammatory infiltration or diffuse tissue inflammation of both neutrophils and lymphocytes) and angiogenesis (number of capillary lumens, congestion, fibrin deposition, and hemorrhage). Both qualitative and quantitative histopathologic scores were taken into consideration and evaluated by two independent pathologists (Kim Min-Kyung Pathology Clinic, Seoul) without knowledge of the previous treatment.

Enzyme-linked immunosorbent assay

The wound tissues were analyzed for cytokine content using the BD OptEIA ELISA set (BD Pharmingen) for the detection of TNF- α , IL-6, IL-1 β and IL-18. All assays were performed as recommended by the manufacturer.

Statistical analysis

Statistical analysis was performed using one-way analysis of variance (ANOVA) followed by Tukey's *post hoc* test using Origin Software (OriginLab 8.0). The statistical significance was set at $P < 0.05$.

Results and discussion

Design of a fibroblast-targeting CPNV_{KTTKS} system

The collagen-derived peptide, KTTKS, a type-1 collagen subfragment with the minimum necessary sequence, has the ability to specifically bind to the PAR-2 receptor on the fibroblast membrane.^{22–24} Taking advantage of this specific interaction, we attempted to establish a smart polymeric nanovehicle (PNV) platform that enables fibroblast-targeted cellular drug delivery for wound healing. To decorate bare PNVs with the KTTKS, we first synthesized a KTTKS-conjugatable lipid linker that can co-assemble with PEO-*b*-PCL during micellization.^{29,32} For this, we employed the MEL as a starting

lipid molecule, in which the hydroxy group in the hydrophilic head was modified with a maleimide group. Consequently, the MEL maleimide linker effectively co-assembled with PEO-*b*-PCL through the hydrophobic interaction between the dialkyl chains and the PCL block, while exposing a maleimide linking site toward the aqueous continuous phase. As the KTTKS has a cysteamine group at the C-terminus, it can be covalently patched on the MEL linker co-assembled with PNVs through a thiol–maleimide reaction. Curcumin was selected as a model active ingredient that can accelerate fibroblast proliferation^{33,34} and was encapsulated in the core, thus producing CPNV_{KTTKS} (Fig. 1a). We expect that CPNV_{KTTKS} would exhibit enhanced cellular uptake through receptor-mediated endocytosis, which would increase the treatment efficiency of curcumin, thus accelerating wound healing (Fig. 1b).

Peripheral engineering of PNV_{KTTKS} for favorable fibroblast targeting

In our PNV_{KTTKS} system, both the KTTKS and PEO blocks were simultaneously oriented toward the aqueous continuous phase. Hence, the fibroblast-targeting ability of KTTKS can be sterically affected in association with the PEO chain conformation. If the PEO block is too short, the cell-targeting performance will increase, but the dispersion stability of the particles may decrease. Conversely, if the length of the PEO block is too long, it may interfere with the exposure of KTTK, thus

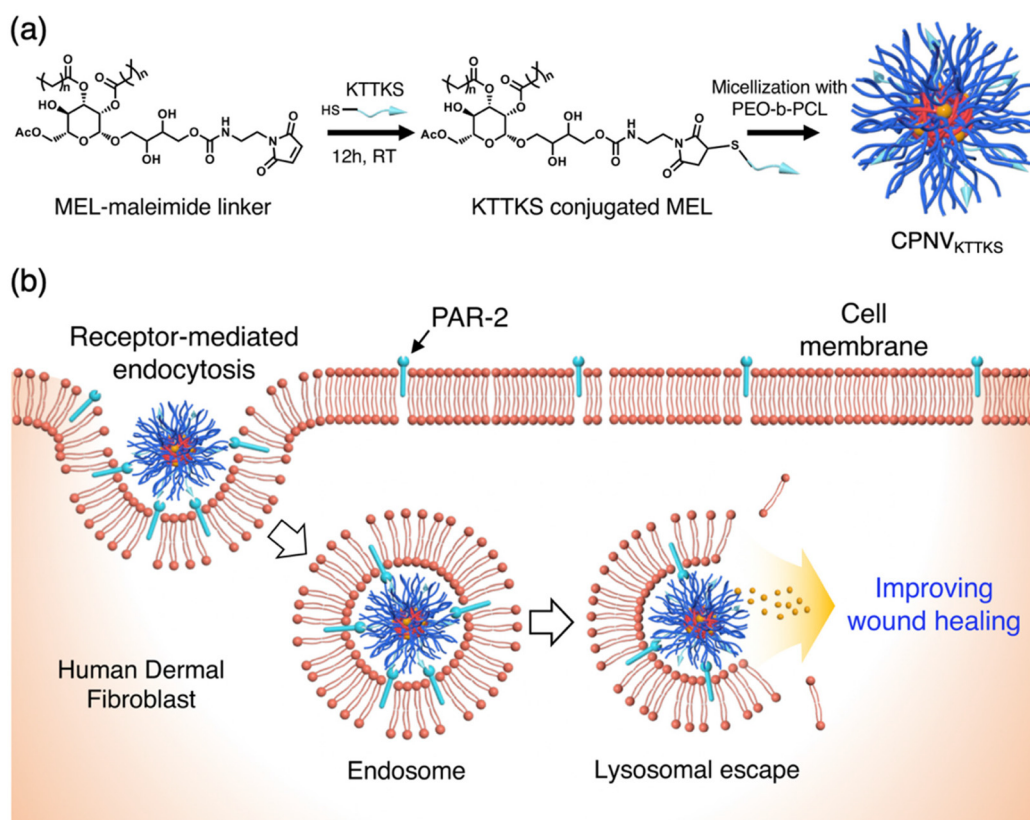


Fig. 1 (a) Fabrication of curcumin-loaded PNV_{KTTKS} (CPNV_{KTTKS}). (b) Schematic illustration of wound healing by CPNV_{KTTKS} through PAR-2 receptor-mediated endocytosis in a fibroblast cell.

deteriorating the cell targeting performance. To experimentally verify this, we prepared $\text{PNV}_{\text{KTTKS}}$ using PEO-*b*-PCL, in which the PEO block length was varied, and tried to confirm how it affects the dispersion stability and fibroblast targeting ability (Fig. 2a). The hydrodynamic particle size of bare PNVs was determined to be approximately 50 nm, and it showed a slightly increasing trend as the KTTKS concentration increased (Fig. 2b). Since KTTKS has a cationic unit, specifically lysine, the zeta potential of $\text{PNV}_{\text{KTTKS}}$ is close to zero. We also confirmed the successful maleimide–thiol reaction between the

MEL linker and KTTKS through ^1H nuclear magnetic resonance (NMR) analysis (Fig. S3†). The difference in the particle sizes of PNVs before and after the KTTKS conjugation was directly confirmed by observing their morphologies by transmission electron microscopy (TEM) (Fig. 2c and d). Even after decorating the KTTKS onto the PNV periphery, a typical polymer micelle morphology was observed, and the particle size increased slightly to the level of several nanometers. Considering the hydration thickness, the particle sizes obtained from the TEM image analysis matched well with

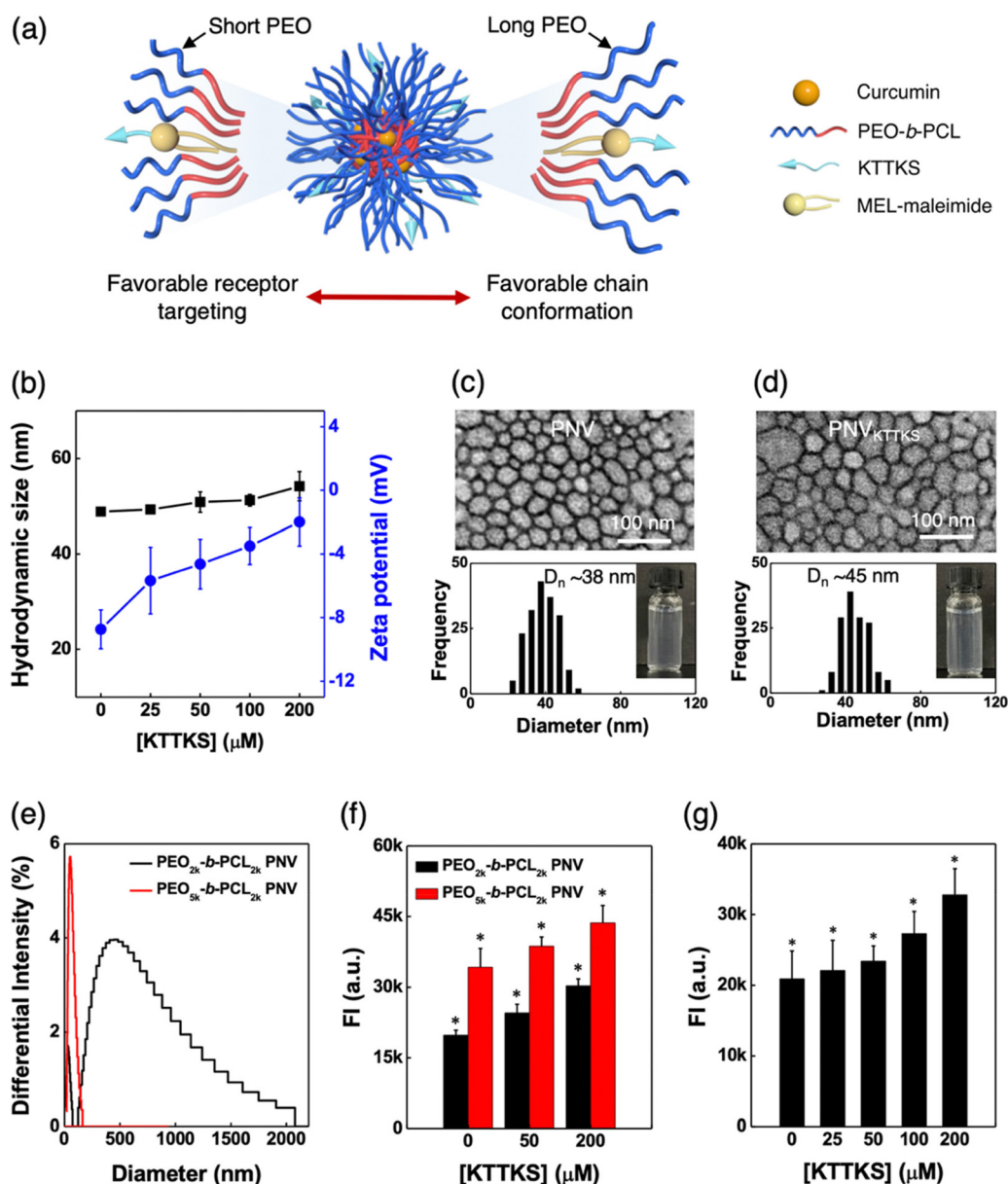


Fig. 2 (a) Competition between receptor targeting and chain conformation on $\text{PNV}_{\text{KTTKS}}$. (b) Hydrodynamic particle size and zeta potential of $\text{PNV}_{\text{KTTKS}}$ upon varying the KTTKS concentration. TEM images and histograms of (c) bare PNVs and (d) $\text{PNV}_{\text{KTTKS}}$. The insets show the actual appearance of bare PNV and $\text{PNV}_{\text{KTTKS}}$ dispersions. $\text{PEO}_{5k}\text{-}b\text{-PCL}_{2k}$ was used in these observations. (e) Hydrodynamic particle size after 24 h from fabrication and (f) quantitative cellular uptake of Nile red-loaded $\text{PNV}_{\text{KTTKS}}$ prepared using PEO-*b*-PCL with different PEO block lengths. (g) Quantitative cellular uptake of Nile red-loaded $\text{PNV}_{\text{KTTKS}}$ prepared by varying the KTTKS concentration. $\text{PEO}_{5k}\text{-}b\text{-PCL}_{2k}$ was used in this case. Error bars represent the standard deviation of the mean ($n = 4$) (* $p < 0.05$, one-way ANOVA).

those determined by dynamic light scattering. These results indicate that although the introduction of KTTKS conferred an association site, it seems to interfere with the chain conformation of the PEO blocks at the PNv surface.

The PNv_{KTTKS} prepared with PEO_{5k}-*b*-PCL_{2k} showed excellent long-term dispersion stability (Fig. S4†). Similarly, the PNv_{KTTKS} prepared with PEO_{2k}-*b*-PCL_{2k} also exhibited stable dispersion with a hydrodynamic particle size of approximately 30 nm immediately after preparation; however, we observed that the particle size increased rapidly over a period of 24 h, resulting in a wide particle size distribution from nanometers to micrometers (Fig. 2e). This seems to be due to the dipole-charge interaction between the methoxy group at the end of the PEO chain and the lysine moiety of KTTKS, which possibly leads to an interparticle association.^{29,35} This deterioration of dispersion stability had a direct effect on the cellular uptake of PNv_{KTTKS}. As the function of KTTKS was blocked and the particle size increased, the PNv_{KTTKS} prepared with PEO_{2k}-*b*-PCL_{2k} showed low cellular uptake regardless of the amount of KTTKS introduced (Fig. 2f). In addition, the approach to zero of the zeta potentials of PNv_{KTTKS} with increasing the KTTKS concentration also caused the dispersion instability, thus lowering the intracellular absorption compared to the bare PNvs. After optimization of the PNv_{KTTKS} incubation time (Fig. S5†), we

observed that the cellular uptake of the PNv_{KTTKS} prepared with PEO_{5k}-*b*-PCL_{2k} in HDF cells increased in a KTTKS-concentration-dependent manner (Fig. 2g). Through these results, we confirmed that although fibroblast targeting and dispersion stability can occur competitively on the PNv_{KTTKS} surface, effective cell delivery can be achieved if cell targeting ability is given in a state where dispersion stability is properly secured.

Direct demonstration of *in vivo* fibroblast targeting performance

The basis of this technology is that PNv_{KTTKS} is selectively delivered only to fibroblasts. To confirm this experimentally, we tried to quantitatively analyze which cell types were more likely to uptake PNv_{KTTKS}, during the co-culture of three types of skin cells, including fibroblasts. The cell mixture was composed of HDF (fibroblast), SK-MEL-28 (melanocyte), and HaCaT (keratinocyte) cells. For better visualization, we prepared Texas red-DHPE-co-assembled PNv_{KTTKS-200} μM. Equal amounts of skin cells (5 × 10⁴ cells per well) were co-cultured in a six-well plate. We normalized the fluorescence intensity of the cells by dividing the detected fluorescence intensity of a cell by the total cell area (Fig. 3a and b). Overall, PNv_{KTTKS} was taken up by all skin cells regardless of the type, because cells always interact with the outer environment by processing

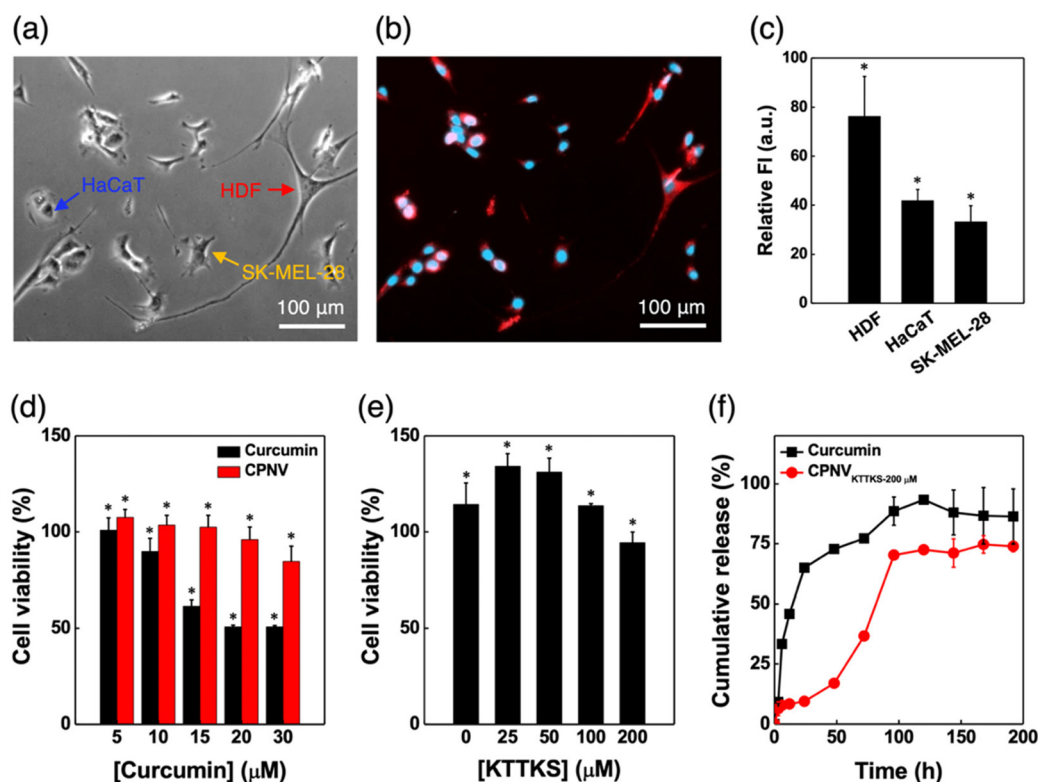


Fig. 3 (a) Optical microscopy image, (b) fluorescence image, and (c) normalized relative fluorescence intensity after incubation with Texas red-DHPE-co-assembled PNv_{KTTKS-200} μM in the skin cell mixture of HDF, HaCaT, and SK-MEL-28 cells. Error bars represent the standard deviation of the mean ($n = 4$) (* $p < 0.05$, one-way ANOVA). (d) Cell viability after 24 h of incubation with CPNV prepared using varying curcumin concentrations. (e) Cell viability after 24 h of incubation with CPNV_{KTTKS} prepared using varying KTTKS concentrations. (f) Release profiles of CPNV_{KTTKS-200} μM in PBS containing 5% v/v Tween-80 at 37 °C. 5 μM curcumin was loaded. Error bars represent the standard deviation of the mean ($n = 6$) (* $p < 0.05$ compared to untreated cells, one-way ANOVA).

passive and active membrane transport. However, PNV_{KTTKS} showed approximately 2-fold higher internalization in HDF cells than in HaCaT and SK-MEL-28 cells (Fig. 3c). These results show that PNV_{KTTKS} exhibits selective cell delivery to fibroblasts, because of the selective interaction with PAR-2 induced by KTTKS. Compared with our previous results,³⁰ our current system introduced a twice higher concentration of KTTKS to PNV_{KTTKS}, however, the fibroblast targeting ability

was similar. This verifies that the fibroblast targeting ability using KTTKS is limited to this level, since the PAR-2 receptors on the HDF cells seem to be saturated by the KTTKS. To increase the fibroblast targeting efficiency, additional conjugation of other ligands capable of targeting receptors such as PDGFR, CD39, or FAP can be considered.

Having established a PNV_{KTTKS} system that can selectively target fibroblasts, our interest shifted to whether fibroblasts can

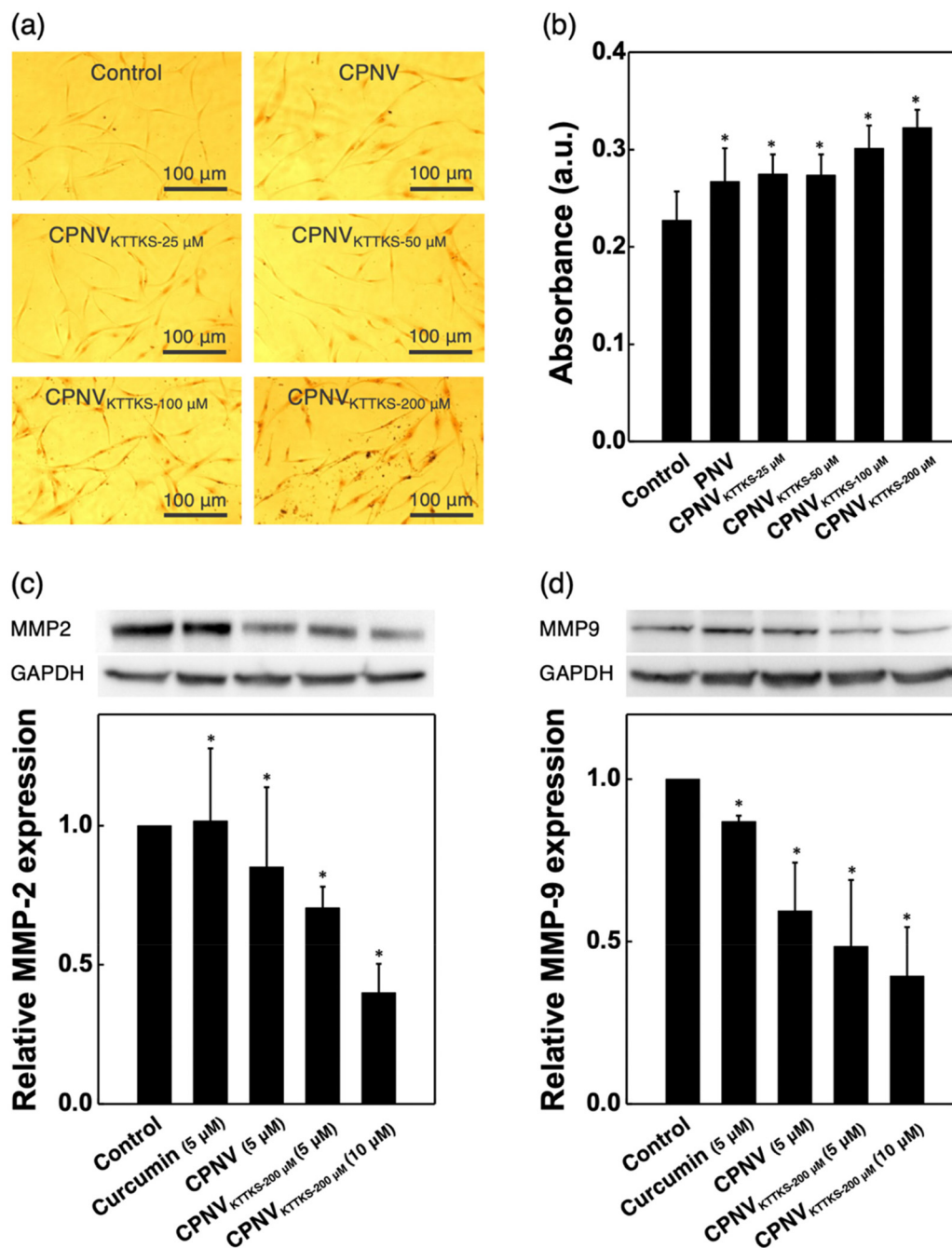


Fig. 4 (a) Microscopic images and (b) comparative quantification of collagen synthesis by HDF cells after treatment with CPNV_{KTTKS} for 24 h. Error bars represent the standard deviation of the mean ($n = 6$). Quantification of the protein levels and relative expressions of (c) MMP-2 and (d) MMP-9, in HDF cells after treatment with CPNV_{KTTKS} for 24 h. The values in parentheses indicate curcumin concentration. Error bars represent the standard deviation of the mean ($n = 3$) (* $p < 0.05$ compared to untreated cells, one-way ANOVA).

be further activated through PNV_{KTTKS}-mediated drug delivery. Curcumin is well-known as a wound healing drug, so we prepared CPNV_{KTTKS} and investigated its ability to activate HDF cells. Because curcumin is cytotoxic, it is difficult to use it at high concentrations.^{36,37} This was confirmed by our cytotoxicity test. In the case of CPNV_{KTTKS}, however, the cytotoxicity of curcumin was significantly lowered. Another interesting observation was that the cell viability was enhanced up to a KTTKS concentration of 100 μM (Fig. 3d). Cytotoxicity has been observed at concentrations above 200 μM (Fig. 3e). These results indicate that the endocytosis of CPNV_{KTTKS} was increased by fibroblast targeting. However, because curcumin is entrapped in the hydrophobic core of CPNV_{KTTKS}, it does not cause cytotoxicity. Moreover, it leads to the sustained release of curcumin, resulting in cell proliferation. When an excess of CPNV_{KTTKS} is administered, the overall amount of curcumin released can be increased, which seems to induce intrinsic cytotoxicity. This interpretation was possible because the sustained release of curcumin from the CPNV_{KTTKS} with a high loading efficiency of 85–90% was observed for several days (Fig. 3f). In the context of fibroblast activation, these advantages of CPNV_{KTTKS} definitely solidify their wound healing applications.

Selective proliferation of fibroblasts for enhanced *in vitro* wound healing

Collagen synthesis and the associated matrix metalloproteinase (MMP) suppression in fibroblasts are very closely linked to the wound healing performance.^{38–41} MMPs are important proteases that are involved in the degradation or cleavage of a wide range of extracellular proteins, especially including collagen and other components of ECM. Therefore, we tried to observe how fibroblast targeting using CPNV_{KTTKS} affects collagen production and MMP expression. To confirm this, HDF cells were

first treated with the CPNV_{KTTKS} prepared with varying KTTKS concentrations for 24 h. After Sirius red staining, the stained collagen molecules were quantified by UV absorbance at 490 nm (Fig. 4a). We observed that CPNV_{KTTKS} enhanced collagen production of HDF cells in a KTTKS-concentration-dependent manner. It showed an increase of 41% compared to the control and 20% compared to bare CPNV, respectively (Fig. 4b). Continuously, we conducted a western blot analysis to confirm the expressions of MMP-2 and 9 in a situation where collagen synthesis is increased by fibroblast targeting of CPNV_{KTTKS} (Fig. 4c and d). Both MMP-2 and 9 expressions in HDF cells were significantly decreased after treatment with CPNV_{KTTKS}. These results support our hypothesis that the fibroblast targeting by CPNV_{KTTKS} plays a role in improving collagen synthesis and related MMP suppression in fibroblasts. In our continued study, we evaluated the wound healing capability of CPNV_{KTTKS} using an *in vitro* scratch assay for HDF cells (Fig. S6†). After 24 h of incubation, the CPNV_{KTTKS} treatment markedly increased the migration of HDF cells to the scratched area, which was comparable to that after treatment with curcumin itself and bare CPNV. After 48 h, the difference became even more pronounced, with most of the scratched area being closed. The loss of cell-to-cell interactions in a wound (or scratch) area results in the expression of growth factors and cytokines, which drives cell migration.⁴² In this process, the CPNV_{KTTKS} promotes collagen production by selective proliferation of fibroblasts, which effectively enhances their migration together with the secretion of growth factors and cytokines, thereby eventually enhancing wound healing.

Remarkable *in vivo* wound healing performance

To verify the *in vivo* wound healing capability of CPNV_{KTTKS}, we observed the macroscopic closure of excisional wounds for 12

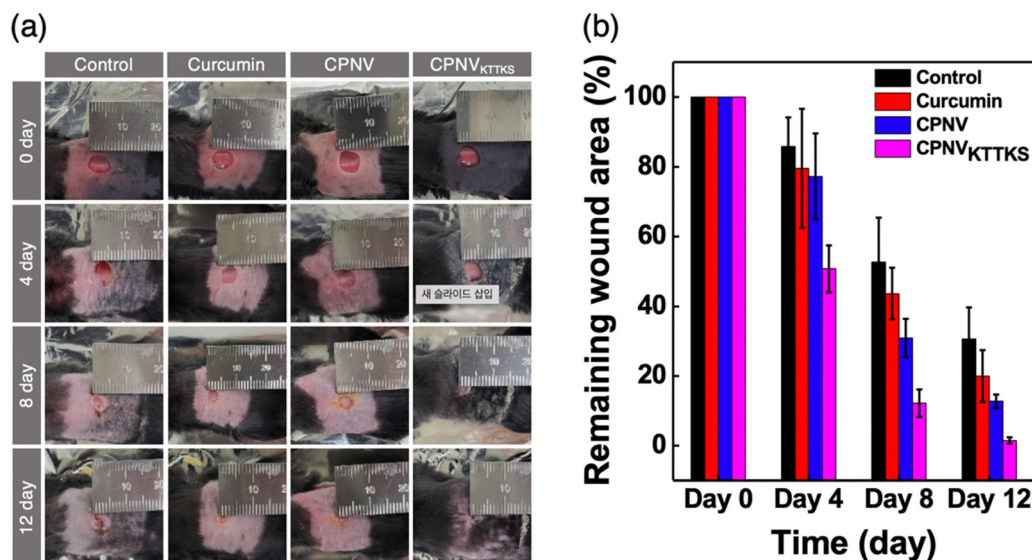


Fig. 5 *In vivo* wound healing activity of CPNVs. (a) Macroscopic observation of excisional CPNV-treated wounds for 12 days. In the control, no treatment was conducted. CPNV_{KTTKS}-200 μM was used in this study. (b) Relative remaining wound area (%) for 12 days after surgery ($n = 4$). Error bars represent the standard deviation of the mean ($n = 4$) (* $p < 0.05$ compared to untreated cells, one-way ANOVA).

days (Fig. 5a and b). It was worthy to note in our study that the CPNV_{KTTKS}-treated wound showed much faster wound closing, which is quite comparable to other cases. Histological analysis of the wound tissues was conducted on the 12th day using

hematoxylin and eosin (H&E) staining and Masson's trichrome (MT) staining (Fig. 6a). The wound tissues treated with CPNV_{KTTKS} presented the regenerated epidermis with focal re-epithelialization and fibroblasts. The semiquantitative histo-

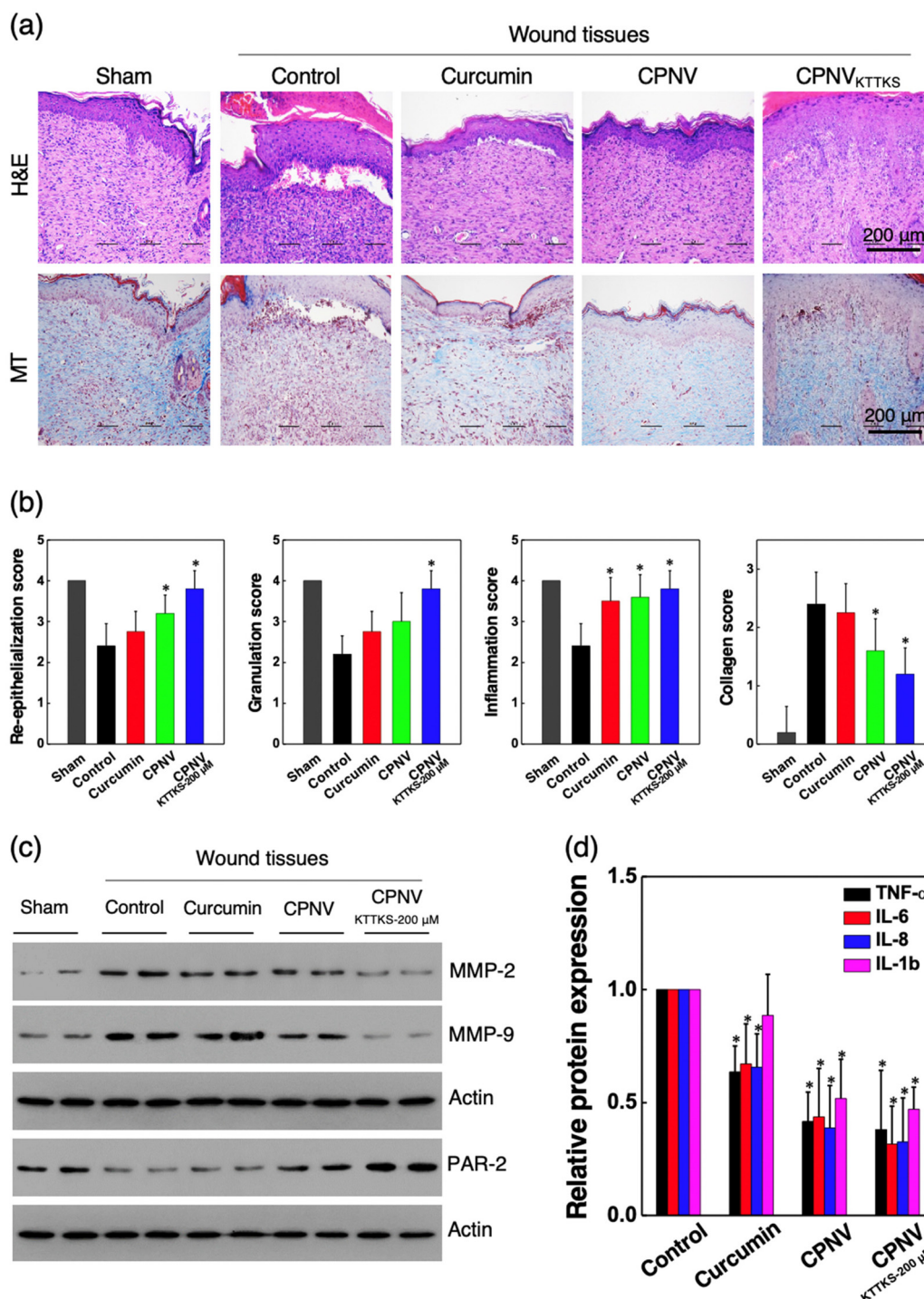


Fig. 6 *In vivo* therapeutic efficacy of CPNVs for tissue wounds. (a) Representative H&E staining (upper) and MT staining (lower) images of wound tissues without (control) and with CPNV or CPNV_{KTTKS-200 μM} treatment on the 12th day ($n = 4$). (b) Levels of re-epithelialization, granulation, inflammatory responses and collagen formed at the wound area were measured according to the pathology criteria (score 0–4) ($n = 4$). (c) Representative expression levels of MMP-2, MMP-9 and PAR-2 at wound tissues on the 12th day. (d) The level of cytokines is analyzed by ELISA for TNF- α , IL-6, IL-8 and IL-1 β ($n = 4$) (* $p < 0.05$ compared to untreated cells, one-way ANOVA).

pathological score of the wound tissues treated with CPNV_{KTTKS}, based on the degree of exposed dermis, re-epithelialization, inflammatory exudate, acute inflammation, fibroblastic migration, and dermal fibrosis, was much greater than that in the other group (Fig. 6b). Additionally, the regeneration and distribution of collagen in the wound tissues were assessed by MT staining during the healing process. The wound tissues treated with CPNV_{KTTKS} showed the highest level of collagen fibril formation during the remodeling process (Fig. 6a and b). Moreover, the CPNV_{KTTKS}-treated wound tissue displayed a moderate level of keratinization, a large area of regenerated dermis, and some follicles, thus significantly contributing to faster and more satisfactory wound healing, which is quite comparable to the cases of using curcumin and CPNV. These results reveal that CPNV_{KTTKS} exhibited excellent therapeutic efficacy for deep wound healing.

Subsequently, the effects of CPNV_{KTTKS} on the pharmacologic and biologic profiles were investigated in wound tissues. Collagen and other components of ECM-associated MMP and PAR-2 receptor-targeted internalization were quantitatively measured in the wound tissues with and without CPNV_{KTTKS} treatment. Consistent with the *in vitro* results (Fig. 1b and 4c, d), CPNV_{KTTKS} treatment markedly decreased the expressions of MMP2 and MMP-9 in the wound tissues and increased the expression of PAR-2 (Fig. 6c), which are close to the level of the sham group. In contrast, the curcumin or CPNV-treated wound tissues presented negligible changes in the expression levels of the MMP and PAR-2, which are similar to the level of the control group without any treatment. Besides, inflammatory cytokines were remarkably reduced in the wound tissue that was treated with CPNV_{KTTKS} (Fig. 6d). These results highlight that the effective targeting of PAR-2 and curcumin delivery of CPNV_{KTTKS} possibly led to such rapid wound healing.

Conclusion

In summary, we developed a fibroblast-targeting PNV system in which the periphery decorated with KTTKS interacted with the PAR-2 receptor on fibroblasts. We experimentally demonstrated that the PNV_{KTTKS} showed improved cellular internalization due to its specific interaction with the PAR-2 receptor. Moreover, PNV_{KTTKS} could be delivered to the targeted fibroblasts with a significant specificity. The essence of our approach was based on the encapsulation of curcumin in the CPNV_{KTTKS}, which dramatically reduced the intrinsic cytotoxicity of curcumin while ensuring sustained release, leading to improved topical wound healing. Based on these findings, we expect that the proposed CPNV_{KTTKS} system has great potential of being developed into a promising drug delivery system for wound healing.

Author contributions

Y. Lee and J. W. Kim conceived and designed the experiments. Y. Lee and S. Kim synthesized the MEL peptide

linker. Y. Lee, J. Seo, and E. J. Park prepared and characterized PNV_{KTTKS} and CPNV_{KTTKS}. Y. Lee and J. O. Park characterized skin cell targeting. H. K. Kim, Y. P. Han and C. S. Yang evaluated *in vivo* wound healing. Y. Lee, C. S. Yang, and J. W. Kim co-wrote the paper. All authors discussed the results and commented on the manuscript.

Conflicts of interest

There are no conflicts to declare.

Acknowledgements

This work was supported by the National Research Foundation of Korea (NRF) grant funded by the Korean government (MSIT) (No. NRF-2021R1A4A1032782 and NRF-2021R1A4A5032463) and by the INNOPOLIS Foundation of Korea (No. 2021-DD-UP-0369).

References

- 1 B. K. Sun, Z. Siplashvili and P. A. Khavari, *Science*, 2014, **346**, 941–945.
- 2 S. A. Eming, P. Martin and M. Tomic-Canic, *Sci. Transl. Med.*, 2014, **6**, 265sr266.
- 3 P. Bainbridge, *J. Wound Care*, 2013, **22**, 407–412.
- 4 L. E. Tracy, R. A. Minasian and E. Caterson, *Adv. Wound Care*, 2016, **5**, 119–136.
- 5 M. L. Zou, Y. Y. Teng, J. J. Wu, S. Y. Liu, X. Y. Tang, Y. Jia, Z. H. Chen, K. W. Zhang, Z. L. Sun, X. Li, J. X. Ye, R. S. Xu and F. L. Yuan, *Front. Cell Dev. Biol.*, 2021, **9**, 9.
- 6 R. T. Hannan, S. M. Peirce and T. H. Barker, *ACS Biomater. Sci. Eng.*, 2017, **4**, 1223–1232.
- 7 S. Saghazadeh, C. Rinoldi, M. Schot, S. S. Kashaf, F. Sharifi, E. Jalilian, K. Nuutila, G. Giatsidis, P. Mostafalu, H. Derakhshandeh, K. Yue, W. Swieszkowski, A. Memic, A. Tamayol and A. Khademhosseini, *Adv. Drug Delivery Rev.*, 2018, **127**, 138–166.
- 8 W. Wang, K. J. Lu, C. H. Yu, Q. L. Huang and Y. Z. Du, *J. Nanobiotechnol.*, 2019, **17**, 82.
- 9 S. Sharifi, M. J. Hajipour, L. Gould and M. Mahmoudi, *Mol. Pharm.*, 2020, **18**, 550–575.
- 10 M. Parani, G. Lokhande, A. Singh and A. K. Gaharwar, *ACS Appl. Mater. Interfaces*, 2016, **8**, 10049–10069.
- 11 T. M. Allen and P. R. Cullis, *Science*, 2004, **303**, 1818–1822.
- 12 V. P. Torchilin, *Nat. Rev. Drug Discovery*, 2014, **13**, 813–827.
- 13 S. Zha, H. F. Chau, W. Y. Chau, L. S. Chan, J. Lin, K. W. Lo, W. C. S. Cho, Y. L. Yip, S. W. Tsao and P. J. Farrell, *Adv. Sci.*, 2021, **8**, 2002919.
- 14 K. Ulbrich, K. Hola, V. Subr, A. Bakandritsos, J. Tucek and R. Zboril, *Chem. Rev.*, 2016, **116**, 5338–5431.
- 15 P. L. Chariou, O. A. Ortega-Rivera and N. F. Steinmetz, *ACS Nano*, 2020, **14**, 2678–2701.

- 16 J. Hwang, M. O. Sullivan and K. L. Kiick, *Front. Bioeng. Biotechnol.*, 2020, **8**, 69.
- 17 C. Zeltz, J. Orgel and D. Gullberg, *Biochim. Biophys. Acta, Gen. Subj.*, 2014, **1840**, 2533–2548.
- 18 B. Leitinger, *Int. Rev. Cell Mol. Biol.*, 2014, **310**, 39–87.
- 19 B. An and B. Brodsky, *Blood*, 2016, **127**, 521–522.
- 20 J. Cichy and E. Puré, *J. Cell Biol.*, 2003, **161**, 839–843.
- 21 R. R. Jones, V. Castelletto, C. J. Connon and I. W. Hamley, *Mol. Pharm.*, 2013, **10**, 1063–1069.
- 22 M. K. Y. Lee, I. D. Kong, J. Ryu, M. Jang, C. Lee and E. H. Choi, *Korean J. Dermatol.*, 2010, **48**, 966–974.
- 23 N. Atrux-Tallau, T. Delmas, S. H. Han, J. W. Kim and J. Bibette, *Int. J. Cosmet. Sci.*, 2013, **35**, 310–318.
- 24 J. H. Cho, J. Y. Kang, S. Kim, H. R. Baek, J. Kim, K. S. Jang and J. W. Kim, *J. Mater. Chem. B*, 2021, **9**, 4956–4962.
- 25 C. D. Spicer, C. Jumeaux, B. Gupta and M. M. Stevens, *Chem. Soc. Rev.*, 2018, **47**, 3574–3620.
- 26 M. Skwarczynski and I. Toth, *Chem. Sci.*, 2016, **7**, 842–854.
- 27 C. Kinnear, T. L. Moore, L. Rodriguez-Lorenzo, B. Rothen-Rutishauser and A. Petri-Fink, *Chem. Rev.*, 2017, **117**, 11476–11521.
- 28 J. H. Lee, J. A. Engler, J. F. Collawn and B. A. Moore, *Eur. J. Biochem.*, 2001, **268**, 2004–2012.
- 29 D. Park, J. Y. Lee, H. K. Cho, W. J. Hong, J. Kim, H. Seo, I. Choi, Y. Lee, J. Kim, S. J. Min, S. H. Yoon, J. S. Hwang, K. J. Cho and J. W. Kim, *Biomacromolecules*, 2018, **19**, 2682–2690.
- 30 J. Y. Kang, S. Kim, J. Kim, N. G. Kang, C. S. Yang, S. J. Min and J. W. Kim, *J. Mater. Chem. B*, 2021, **9**, 464–470.
- 31 S. D'Souza, *Adv. Pharm.*, 2014, **2014**, 12.
- 32 S. Hong, J. Park, J. E. Kim, D. Park, S. Kim, J. Y. Kang, J. Y. Lee, W. J. Hong, H. Jeon and H. Lee, *Int. J. Pharm.*, 2019, **565**, 233–241.
- 33 P. Zhou, H. Zhou, J. Shu, S. Fu and Z. Yang, *Ann. Transl. Med.*, 2021, **9**, 1152.
- 34 Z. Song, Y. Wen, F. Teng, M. Wang, N. Liu and R. Feng, *New J. Chem.*, 2022, **46**, 3674–3686.
- 35 K. Shin, G. Gong, J. Cuadrado, S. Jeon, M. Seo, H. S. Choi, J. S. Hwang, Y. Lee, A. Fernandez-Nieves and J. W. Kim, *Chem. – Eur. J.*, 2017, **23**, 4292–4297.
- 36 P. S. Mandrol, K. Bhat and A. Prabhakar, *J. Indian Soc. Pedod. Prev. Dent.*, 2016, **34**, 269.
- 37 A. Scharstuhl, H. Mutsaers, S. Pennings, W. Szarek, F. Russel and F. Wagener, *J. Cell. Mol. Med.*, 2009, **13**, 712–725.
- 38 S. S. Mathew-Steiner, S. Roy and C. K. Sen, *Bioengineering*, 2021, **8**, 63.
- 39 K. Gelse, E. Pöschl and T. Aigner, *Adv. Drug Delivery Rev.*, 2003, **55**, 1531–1546.
- 40 Y. Liu, D. Min, T. Bolton, V. Nubé, S. M. Twigg, D. K. Yue and S. V. McLennan, *Diabetes Care*, 2009, **32**, 117–119.
- 41 S. M. McCarty and S. L. Percival, *Adv. Wound Care*, 2013, **2**, 438–447.
- 42 C.-C. Liang, A. Y. Park and J.-L. Guan, *Nat. Protoc.*, 2007, **2**, 329–333.